

01,05

Structure and magnetic properties of amorphous and nanocrystalline Co-Fe-B-(Nb, Ti) alloys

© V.V. Chirkova, N.A. Volkov, I.A. Sholin, G.E. Abrosimova, A.S. Aronin

Osipyan Institute of Solid State Physics RAS,
Chernogolovka, Russia

E-mail: valyffkin@issp.ac.ru

Received March 9, 2022

Revised March 9, 2022

Accepted March 10, 2022

The structure and magnetic properties of amorphous and nanocrystalline $\text{Co}_{56}\text{Fe}_{16}\text{B}_{20}\text{X}_8$ ($X = \text{Nb, Ti}$) alloys have been studied by X-ray diffraction and vibrating sample magnetometry. It is shown that the saturation magnetization of the amorphous $\text{Co}_{56}\text{Fe}_{16}\text{B}_{20}\text{Ti}_8$ alloy is higher than that of the $\text{Co}_{56}\text{Fe}_{16}\text{B}_{20}\text{Nb}_8$ alloy. The temperature dependence of the saturation magnetization of amorphous alloys is measured and it is shown that the saturation magnetization of the $\text{Co}_{56}\text{Fe}_{16}\text{B}_{20}\text{Ti}_8$ alloy decreases with temperature more slowly than the magnetization of the $\text{Co}_{56}\text{Fe}_{16}\text{B}_{20}\text{Nb}_8$ alloy. Crystallization of amorphous alloys leads to a decrease in the saturation magnetization of both alloys. During crystallization, BCC nanocrystals are formed in the $\text{Co}_{56}\text{Fe}_{16}\text{B}_{20}\text{Nb}_8$ alloy and multiphase structure is formed in the $\text{Co}_{56}\text{Fe}_{16}\text{B}_{20}\text{Ti}_8$ alloy.

Keywords: amorphous phase, crystallization, nanocrystals, magnetic properties.

DOI: 10.21883/PSS.2022.07.54578.307

1. Introduction

Creation of promising materials with unique physical properties is an integral part of scientific and technological progress. In connection with the constant development of radio and microelectronics, it is especially important to develop materials that are distinguished by good magnetic properties. These include amorphous alloys based on iron and cobalt [1–4]. These materials have high saturation magnetization, high magnetic permeability, low coercivity, low remagnetization loss and other good soft magnetic properties [5–11].

The magnetic properties of amorphous alloys can be improved by forming an amorphous-nanocrystalline structure consisting of nanocrystals distributed in an amorphous matrix. There are various ways to obtain a nanocrystalline structure [12–16]. One of the most commonly used methods is the controlled crystallization of the amorphous phase, which is carried out using heat treatment. Since not all amorphous alloys crystallize with the formation of nanocrystals during heat treatment, alloying components are added to the alloy, which increase the rate of crystal nucleation and decrease the rate of their growth [17–20]. The first nanocrystalline alloy produced in this way was an Fe-Si-B alloy alloyed with Cu and Nb, called Finemet ($\text{Fe}_{73.5}\text{Si}_{13.5}\text{B}_9\text{Nb}_3\text{Cu}_1$) [21]. During the formation of a nanostructure in an amorphous $\text{Fe}_{73.5}\text{Si}_{13.5}\text{B}_9\text{Nb}_3\text{Cu}_1$ alloy, there is an increase in magnetic permeability and a decrease in remagnetization losses [22].

Introduction of alloying components can affect the magnetic properties in different ways [23–25]. For example, addition of Fe to cobalt-based amorphous alloys increases

the saturation magnetization and reduces the coercivity [26], while adding Pt to amorphous alloys of the Co-Si-B system, a decrease in saturation magnetization is observed [27].

Cobalt-based amorphous alloys are characterized by a lower saturation magnetization compared to iron-based alloys, but a higher Curie temperature [28], which determines the prospects for using these magnetic materials at elevated temperatures. To create materials with a complex of good functional properties, it is necessary to know the conditions for formation of structures that provide high properties, their dependence on the chemical composition and processing conditions. Currently, there are many articles devoted to the study of the influence of alloying components on the structure and properties of amorphous and partially crystalline alloys of different compositions [29–32], however, there are practically no articles that study alloys with the same concentration of base and alloying components that differ only in the type of alloying component. In this article, $\text{Co}_{56}\text{Fe}_{16}\text{B}_{20}\text{X}_8$ ($X = \text{Nb, Ti}$) alloys with the same concentration of basic and alloying components were studied.

2. Materials and methods

Amorphous alloys $\text{Co}_{56}\text{Fe}_{16}\text{B}_{20}\text{X}_8$ ($X = \text{Nb, Ti}$) were obtained in the form of ribbons melt spinning on a fast-moving substrate. The cooling rate was 10^6 K/s. The width of the obtained ribbons was about 1 cm, and their thickness was $40\ \mu\text{m}$. The composition of the alloys was controlled by local X-ray microanalysis using a Zeiss Supra 50VP scanning electron microscope. Determination of the crystallization temperature and phase transformation temperatures

was carried out using a Perkin-Elmer 7 differential scanning calorimeter, the heating rate was 20 K/min. The initial amorphous samples were also subjected to isothermal annealing at temperatures of 673–823 K in a resistance furnace. To prevent oxidation during annealing, the samples were placed in a carbon container.

The structure of the initial and annealed samples was studied by X-ray diffraction analysis on Siemens D-500 X-ray diffractometer using Co K_{α} -radiation. During the study, the samples were placed on a special substrate that does not give its own reflections [33]. When processing the spectra, programs were used that enabled to carry out smoothing, background correction, and separation of overlapping maxima. Analysis of X-ray diffraction patterns and identification of phases formed after heat treatment were carried out using the JCPDS database.

The magnetic properties of the samples were studied using a P.A.R. (Princeton Applied Research Model 155) vibrating magnetometer. The saturation magnetization and the coercivity of the studied samples at room temperature were determined using the hysteresis curves. The study of the temperature dependence of the amorphous alloys saturation magnetization was carried out at temperatures of 293–673 K using a high-temperature attachment to a vibrating magnetometer. To do this, the samples under study were placed in a special holder, which was installed inside the high-temperature attachment. After reaching the required temperatures and keeping the samples at these temperatures for ~ 5 min, the hysteresis curves were measured. The hysteresis curves were measured at temperatures of 293, 373 K and then with a step of 50 K up to a temperature of 673 K.

3. Results and discussion

The alloys under study were amorphous after preparation. There were no diffraction reflections from crystalline phases in the X-ray patterns, and only an amorphous halo was observed. According to previous studies [34], the crystallization start temperature of $\text{Co}_{56}\text{Fe}_{16}\text{B}_{20}\text{Nb}_8$ (1) and $\text{Co}_{56}\text{Fe}_{16}\text{B}_{20}\text{Ti}_8$ (2) is 763 and 733 K, respectively. The study of the temperature dependence of the saturation magnetization of the initial amorphous alloys was carried out in a temperature range not exceeding the crystallization start temperature.

Figure 1 shows the temperature dependences of the saturation magnetization of amorphous $\text{Co}_{56}\text{Fe}_{16}\text{B}_{20}\text{Nb}_8$ alloys (squares) and $\text{Co}_{56}\text{Fe}_{16}\text{B}_{20}\text{Ti}_8$ (circles) in reduced units. For comparison with the alloys under study, Figure 1 also shows the temperature dependences of the saturation magnetization of two amorphous iron-based alloys. The temperature dependence of the magnetization of the $\text{Fe}_{80}\text{Si}_6\text{B}_{14}$ alloy was constructed based on the data of the article [35], and the temperature dependence of the saturation magnetization of the $\text{Fe}_{70}\text{Si}_{13}\text{B}_{13}\text{Cu}_1\text{Nb}_3$ amorphous alloy — according to

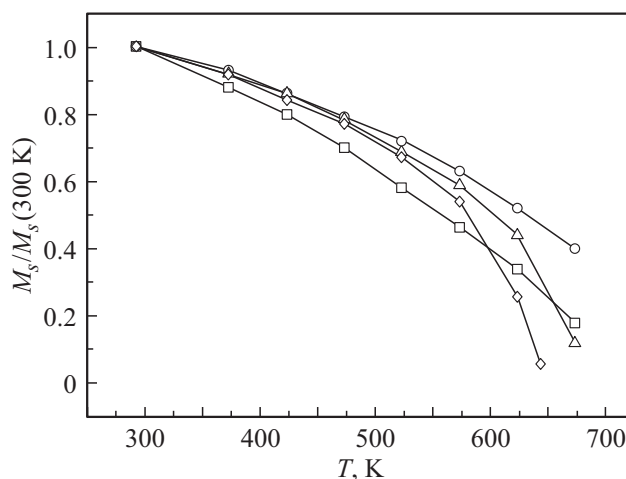


Figure 1. Temperature dependence of saturation magnetization of $\text{Co}_{56}\text{Fe}_{16}\text{B}_{20}\text{Nb}_8$ (squares), $\text{Co}_{56}\text{Fe}_{16}\text{B}_{20}\text{Ti}_8$ (circles), $\text{Fe}_{80}\text{Si}_6\text{B}_{14}$ (triangles), $\text{Fe}_{70}\text{Si}_{13}\text{B}_{13}\text{Cu}_1\text{Nb}_3$ (diamonds) alloys in reduced units.

article [36]. In Fig. 1, these dependencies are represented by triangles and diamonds, respectively.

It can be seen that the reduced saturation magnetization of the $\text{Co}_{56}\text{Fe}_{16}\text{B}_{20}\text{Ti}_8$ alloy decreases more slowly with increasing temperature than the magnetization of the $\text{Co}_{56}\text{Fe}_{16}\text{B}_{20}\text{Nb}_8$ alloy. For iron-based alloys, approximately the same behavior of saturation magnetization is observed as for an alloy alloyed with titanium. However, above 475 K, the magnetization of iron-based alloys begins to decrease faster than that of the $\text{Co}_{56}\text{Fe}_{16}\text{B}_{20}\text{Ti}_8$. Compared to iron-based alloys, in the $\text{Co}_{56}\text{Fe}_{16}\text{B}_{20}\text{Nb}_8$ alloy at temperatures of 300–575 K, a more rapid decrease in the magnetization is observed. But already at higher temperatures (~ 625 K), the saturation magnetization of this alloy begins to fall more slowly.

At room temperature, the saturation magnetization of the $\text{Co}_{56}\text{Fe}_{16}\text{B}_{20}\text{Nb}_8$ and $\text{Co}_{56}\text{Fe}_{16}\text{B}_{20}\text{Ti}_8$ amorphous alloys determined using the hysteresis curves are 80 and 94 emu/g, respectively. At the same time, as mentioned above, iron-based alloys have a higher saturation magnetization than cobalt-based alloys. For example, amorphous alloys of the Finemet type at room temperature have saturation magnetization of approximately 130–150 emu/g [37,38], which is noticeably higher than magnetization of the cobalt-based alloys under study. Although iron-based amorphous alloys have a high saturation magnetization at room temperature, their magnetization, compared to cobalt-based alloys, changes more strongly with temperature, as can be seen in Fig. 1.

Almost all iron-based amorphous alloys show high saturation magnetization at room temperature [39–42]. However, depending on the composition, magnetization of these alloys can drop so much with temperature that it turns out to be below the saturation magnetization of cobalt-based alloys. For example, in the article [43] the $\text{Fe}_{78}\text{Si}_9\text{B}_{13}$ amorphous alloy at temperature ~ 675 K has a

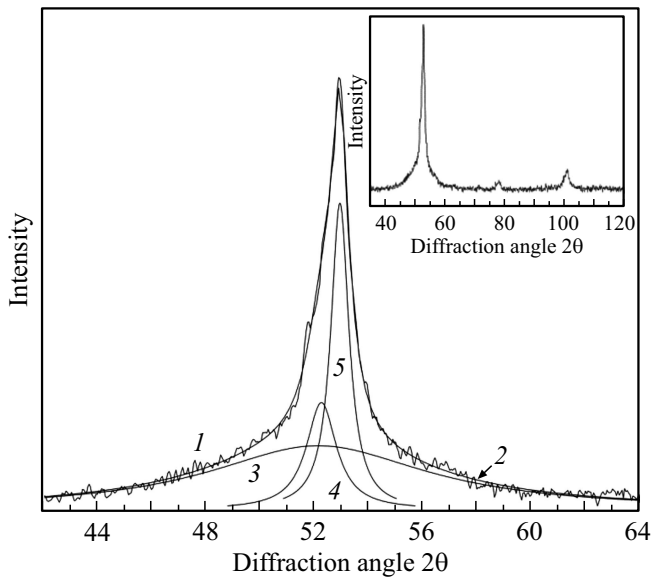


Figure 2. X-ray diffraction pattern of the $\text{Co}_{56}\text{Fe}_{16}\text{B}_{20}\text{Nb}_8$ alloy after isothermal annealing at temperature of 823 K for 1 h (1 — experimental curve, 2 — total curve, 3 — scattering from amorphous phase, 4 — reflection from the FCC Co crystalline phase, 5 — reflection from the BCC crystalline phase).

magnetization of 27 emu/g. At the same time, the saturation magnetization of the $\text{Co}_{80}\text{Si}_6\text{B}_{14}$ amorphous alloy, studied in the article [44], at the same temperature is 79 emu/g, i.e. at elevated temperatures, amorphous cobalt-based alloys can have higher saturation magnetization values than iron-based alloys.

Thus, the saturation magnetization of the studied alloys depends on their chemical composition. Replacement of the alloying component of niobium with titanium in cobalt-based alloys leads to an increase in the saturation magnetization. In this case, the saturation magnetization of the alloy alloyed with titanium depends on temperature to a lesser extent. This behavior of the saturation magnetization of cobalt-based alloys can be used in those cases where studies are required at elevated temperatures.

It is natural to compare the magnetic properties of alloys in the amorphous and partially crystalline states, when the structure consists of nanocrystals randomly distributed in the amorphous phase. To do this, the alloys were annealed at different temperatures, at which a composite amorphous-crystalline structure was formed. Figures 2 and 3 show X-ray diffraction patterns of annealed alloys $\text{Co}_{56}\text{Fe}_{16}\text{B}_{20}\text{Nb}_8$ and $\text{Co}_{56}\text{Fe}_{16}\text{B}_{20}\text{Ti}_8$. Both figures show the regions of the main diffuse maximum, and the insets show full X-ray diffraction patterns. It can be seen that the structure formed at the initial stage of crystallization depends significantly on the type of alloying component.

The general view of the X-ray diffraction pattern of the $\text{Co}_{56}\text{Fe}_{16}\text{B}_{20}\text{Nb}_8$ alloy (Fig. 2, inset) indicates the existence of two phases: an amorphous one (a pedestal under the main maximum) and a phase with BCC structure (the

angular positions of the observed peaks correspond to the (110), (200), and (211) reflections of the cubic phase). However, the analysis of the shape of the maxima showed that the structure is more complex and, in addition to the amorphous phase, the sample contains precipitates of two crystalline cubic phases: with face-centered and body-centered lattices. The figure shows a diffuse halo from the amorphous phase (curve 3) and diffraction reflections from the BCC-phase (curve 5) and FCC-phases (curve 4). The total curve (2) curve representing the sum of 3, 4 and 5 curves coincides with the experimental curve (1). The FCC-phase is a precipitate of the high-temperature modification of Co, and the BCC-phase is a solid solution of the alloy components. Such a phase was also observed earlier in these alloys [45]. It can be seen that the (110) reflection of the BCC-phase is noticeably more intense than the (111) FCC-Co reflection. An analysis of the intensities of all reflections showed that the dominant crystalline phase is the phase with the BCC lattice.

During crystallization of the $\text{Co}_{56}\text{Fe}_{16}\text{B}_{20}\text{Ti}_8$ amorphous alloy, four crystalline phases are formed (Fig. 3). In addition to the amorphous phase, the samples contain crystals of the Co_{23}B_6 type phase, high-temperature modification of cobalt (FCC), Co_3B phase, and a small amount of BCC-phase. It should be noted that the most intense line (110) of the BCC-phase coincides with the most intense line (031) of the Co_3B phase. As can be seen, there are other overlapping lines. The conclusion about the presence of all listed phases was made on the basis of the analysis of X-ray diffraction patterns, taking into account the intensities and half-widths of the diffraction lines.

It should also be noted that after an hourly annealing at 823 K, the fraction of the crystalline component in the studied alloys is different. In the alloy alloyed with titanium,

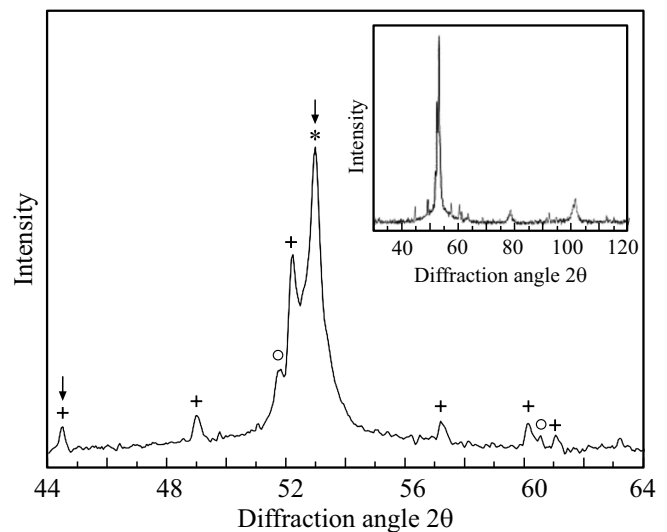


Figure 3. X-ray diffraction pattern of the $\text{Co}_{56}\text{Fe}_{16}\text{B}_{20}\text{Ti}_8$ alloy after isothermal annealing at temperature of 823 K for 1 h (asterisk — BCC phase, crosses — Co_{23}B_6 , circles — fcc-Co, arrows — Co_3B).

Magnetic properties of alloys $\text{Co}_{56}\text{Fe}_{16}\text{B}_{20}\text{Nb}_8$ and $\text{Co}_{56}\text{Fe}_{16}\text{B}_{20}\text{Ti}_8$

Heat Treatment	Alloy Composition	Saturation Magnetization, emu/g	Coercivity, Oe
Initial amorphous alloys	$\text{Co}_{56}\text{Fe}_{16}\text{B}_{20}\text{Nb}_8$	80	< 0.5
	$\text{Co}_{56}\text{Fe}_{16}\text{B}_{20}\text{Ti}_8$	94	< 0.5
Fraction of the crystalline phase less than 5%	$\text{Co}_{56}\text{Fe}_{16}\text{B}_{20}\text{Nb}_8$	77	≤ 1
	$\text{Co}_{56}\text{Fe}_{16}\text{B}_{20}\text{Ti}_8$	85	4
Partially crystalline samples	$\text{Co}_{56}\text{Fe}_{16}\text{B}_{20}\text{Nb}_8$	73	44
	$\text{Co}_{56}\text{Fe}_{16}\text{B}_{20}\text{Ti}_8$	85	63

the fraction of the crystalline component is by 1.2 times greater than in the alloy alloyed with niobium, which is due to the lower crystallization temperature of the $\text{Co}_{56}\text{Fe}_{16}\text{B}_{20}\text{Ti}_8$ alloy.

Thus, after the first stage of crystallization, the structure of the alloys noticeably differs. Measurements of the magnetic properties of partially crystalline alloys (after annealing at 823 K) showed that the values of the saturation magnetization and coercivity also turn out to be different. Figures 4, 5 show the hysteresis curves of $\text{Co}_{56}\text{Fe}_{16}\text{B}_{20}\text{Nb}_8$ and $\text{Co}_{56}\text{Fe}_{16}\text{B}_{20}\text{Ti}_8$ alloys after isothermal annealing. The determined values of the saturation magnetization and the coercivity of the partially crystalline alloy $\text{Co}_{56}\text{Fe}_{16}\text{B}_{20}\text{Nb}_8$ are 73 emu/g and 44 Oe, respectively. For the partially crystalline alloy $\text{Co}_{56}\text{Fe}_{16}\text{B}_{20}\text{Ti}_8$, the same values are 85 emu/g and 63 Oe. The saturation magnetization of the alloy alloyed with niobium is lower than that of the alloy alloyed with titanium.

It was previously found that the initial stage of crystallization of the $\text{Co}_{56}\text{Fe}_{16}\text{B}_{20}\text{Ti}_8$ amorphous alloy is more complex, the above phases are not formed simultaneously. At the very initial stage of crystallization, a small amount of the BCC-phase is formed, and then all other phases are formed. On the DSC curves, this process corresponds to one maximum, however, if the crystallization process is stopped at an early stage, it is possible to obtain samples containing only an amorphous phase and nanocrystals with a BCC structure [34]. With the use of such treatment, samples of the $\text{Co}_{56}\text{Fe}_{16}\text{B}_{20}\text{Ti}_8$ and $\text{Co}_{56}\text{Fe}_{16}\text{B}_{20}\text{Nb}_8$ alloys containing about 5% of the crystalline phase were obtained.

The saturation magnetization of the $\text{Co}_{56}\text{Fe}_{16}\text{Nb}_8\text{B}_{20}$ alloy after such heat treatment is 77 emu/g and decreases to 73 emu/g after the end of the first stage of crystallization. The saturation magnetization of the crystallized alloy $\text{Co}_{56}\text{Fe}_{16}\text{B}_{20}\text{Ti}_8$ is 85 emu/g and does not change with an increase in the fraction of the crystalline phase. After the end of the first stage of crystallization, the coercivities of the alloys increase. It should be noted that the method of vibrational magnetometry does not allow for accurate measurement of the coercivity of amorphous alloys; it turns out to be higher than the real values. For a more accurate determination of the coercivity of alloys containing less than 5% of the fraction of the crystalline phase, additional

experiments were carried out at lower values of the applied magnetic field. The results obtained are shown in the table.

Thus, with the same percentage of components, the alloy alloyed with titanium ($\text{Co}_{56}\text{Fe}_{16}\text{B}_{20}\text{Ti}_8$), is characterized by

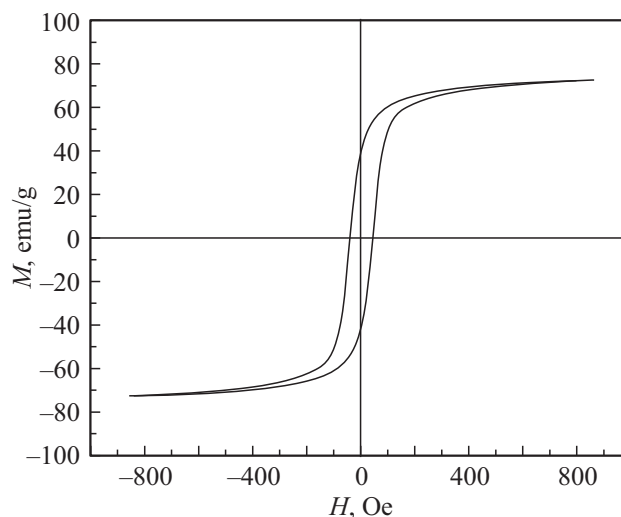


Figure 4. Hysteresis curve of $\text{Co}_{56}\text{Fe}_{16}\text{B}_{20}\text{Nb}_8$ alloy after isothermal annealing at 823 K for 1 h.

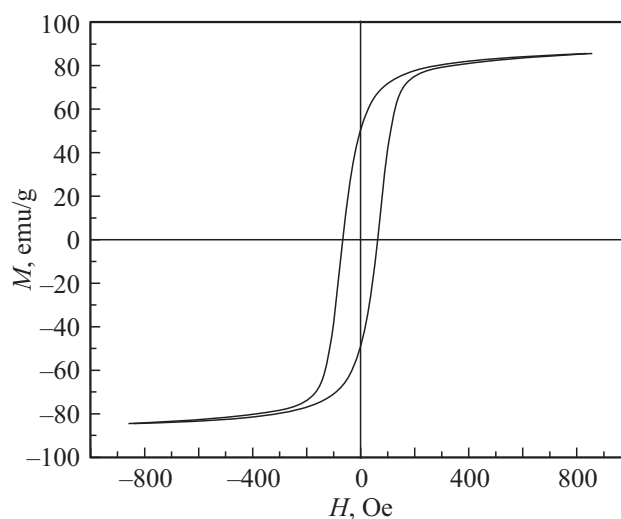


Figure 5. Hysteresis curve of $\text{Co}_{56}\text{Fe}_{16}\text{B}_{20}\text{Ti}_8$ alloy after isothermal annealing at 823 K for 1 h.

a higher value of saturation magnetization compared to the alloy alloyed with niobium ($\text{Co}_{56}\text{Fe}_{16}\text{B}_{20}\text{Nb}_8$).

4. Conclusion

Study of the influence of alloying components on the structure and magnetic properties of amorphous and partially crystalline alloys $\text{Co}_{56}\text{Fe}_{16}\text{B}_{20}\text{X}_8$ ($\text{X} = \text{Nb, Ti}$) showed that

- $\text{Co}_{56}\text{Fe}_{16}\text{B}_{20}\text{Ti}_8$ amorphous alloy has a higher saturation magnetization than $\text{Co}_{56}\text{Fe}_{16}\text{B}_{20}\text{Nb}_8$ alloy;
- decrease in saturation magnetization of $\text{Co}_{56}\text{Fe}_{16}\text{B}_{20}\text{Nb}_8$ and $\text{Co}_{56}\text{Fe}_{16}\text{B}_{20}\text{Ti}_8$ amorphous alloys with increasing temperature is slower than the decrease in the saturation magnetization of iron-based alloys;
- crystallization of amorphous alloys leads to a decrease in the saturation magnetization of $\text{Co}_{56}\text{Fe}_{16}\text{B}_{20}\text{Nb}_8$ and $\text{Co}_{56}\text{Fe}_{16}\text{B}_{20}\text{Ti}_8$ alloys, and with an increase in the fraction of crystalline phases, the saturation magnetization of the $\text{Co}_{56}\text{Fe}_{16}\text{B}_{20}\text{Nb}_8$ alloy decreases; magnetization of $\text{Co}_{56}\text{Fe}_{16}\text{B}_{20}\text{Ti}_8$ does not change;
- after isothermal annealing in the $\text{Co}_{56}\text{Fe}_{16}\text{B}_{20}\text{Nb}_8$ alloy, a phase with a BCC structure and a high-temperature modification of Co are formed; in the $\text{Co}_{56}\text{Fe}_{16}\text{B}_{20}\text{Ti}_8$ alloy, a multiphase crystal structure is formed.

Funding

The studies were carried out within the scope of the state assignment of ISSP RAS.

Conflict of interest

The authors declare that they have no conflict of interest.

References

- [1] M.E. McHenry, M.A. Willard, D.E. Laughlin. *Prog. Mater. Sci.* **44**, 4, 291 (1999). [https://doi.org/10.1016/S0079-6425\(99\)00002-X](https://doi.org/10.1016/S0079-6425(99)00002-X)
- [2] B. Hernando, M.L. Sánchez, V.M. Prida, M. Tejedor, M. Vázquez. *J. Appl. Phys.* **90**, 9, 4783 (2001). <http://dx.doi.org/10.1063/1.1408594>
- [3] G. Herzer. *Acta Mater.* **61**, 3, 718, (2013). <https://doi.org/10.1016/j.actamat.2012.10.040>
- [4] C. Morón, C. Cabrera, A. Morón, A. García, M. González. *Sensors* **15**, 11, 28340 (2015). <http://dx.doi.org/10.3390/s151128340>
- [5] R. Xiang, Sh. Zhou, B. Dong, G. Zhang, Z. Li, Y. Wang, Ch. Chang. *Progr. In Natural Sci. Mater. Int.* **24**, 6, 649 (2014). <http://dx.doi.org/10.1016/j.pnsc.2014.10.002>
- [6] C.F. Conde, J.S. Blazquez, A. Conde. In: *Properties and Application of Nanocrystalline Alloys from amorphous Precursor* / Ed. B. Idzikowski. Kluwer Academic Publ., The Netherlands 184 (2005). P. 111.
- [7] V. Chunchu, G. Markandeyulu. *J. Appl. Phys.* **113**, 17, 17A321 (2013). <https://doi.org/10.1063/1.4795800>
- [8] G.E. Abrosimova, A.S. Aronin, Yu.P. Kabanov, D.V. Matveev, V.V. Molokanov. *FTT* **46**, 5, 858 (2004) (in Russian). <https://doi.org/10.1134/1.1744967>
- [9] G.E. Abrosimova, A.S. Aronin, Yu.P. Kabanov, D.V. Matveev, V.V. Molokanov, O.G. Rybchenko. *FTT* **46**, 12, 2158 (2004) (in Russian). <https://doi.org/10.1134/1.1841387>
- [10] V. Cremaschi, B. Arcondo, H. Sirkin, M. Vazquez, A. Asenjo, J.M. Garcia, G. Abrosimova, A. Aronin. *J. Mater. Res.* **15**, 9, 1936 (2000). <https://doi.org/10.1557/JMR.2000.0279>
- [11] M. Ohta, Y. Yoshizawa. *Jpn. J. Appl. Phys.* **46**, 6L, 062517 (2007). <http://dx.doi.org/10.1143/JJAP.46.L477>
- [12] Zs. Kovács, P. Henits, S. Hobor, A. Révész. *Rev. Adv. Mater. Sci.*, **18**, 7, 593 (2008). https://www.ipme.ru/e-journals/RAMS/no_71808/kovacs.pdf
- [13] G. Abrosimova, A. Aronin, O. Barkalov, D. Matveev, O. Rybchenko, V. Maslov, V. Tkach. *FTT* **53**, 2, 215 (2011) (in Russian). <https://doi.org/10.1134/S1063783411020028>
- [14] A.N. Petrova, I.G. Brodova, O.A. Plekhov, O.B. Naimark, E.V. Shorokhov. *ZhTF* **84**, 7, 44 (2014) (in Russian). <https://doi.org/10.1134/S1063784214070226>
- [15] G.E. Abrosimova, A.S. Aronin, N.A. Volkov. *FTT* **61**, 7, 1352 (2019) (in Russian). <https://doi.org/10.21883/FTT.2019.07.47850.415>
- [16] N.N. Sitnikov, A.V. Shelyakov, R.V. Sundeev, I.A. Khabibulina. *FTT* **62**, 5, 649 (2020) (in Russian). <https://doi.org/10.21883/FTT.2020.05.49223.14M>
- [17] G. Abrosimova, N. Volkov, N. Orlova, A. Aronin. *Mater. Lett.* **219**, 97 (2018). <https://doi.org/10.1016/j.matlet.2018.02.069>
- [18] A. Makino, T. Bitoh, A. Inoue, T. Masumoto. *J. Appl. Phys.* **81**, 6, 2736 (1997). <http://dx.doi.org/10.1063/1.363976>
- [19] K. Hono, K. Hiraga, Q. Wang, A. Inoue, T. Sakurai. *Acta Met. Mater.* **40**, 9, 2137 (1992). [https://doi.org/10.1016/0956-7151\(92\)90131-W](https://doi.org/10.1016/0956-7151(92)90131-W)
- [20] H.A. Shivaee, A. Castellero, P. Rizzi, P. Tiberto, H. Hosseini, M. Baricco. *Met. Mater. Int.* **19**, 4, 643 (2013). <https://doi.org/10.1007/s12540-013-4003-9>
- [21] Y. Yoshizawa, S. Oguma, K. Yamauchi. *J. Appl. Phys.* **64**, 10, 6044 (1988). <https://doi.org/10.1063/1.342149>
- [22] G. Herzer. In: *Magnetic Hysteresis in Novel Materials* / Ed. G.C. Hadjipanayis. Kluwer Academic Publ., The Netherlands 338 (1997). P. 711.
- [23] J. Han, J. Hong, S. Kwon, H. Choi-Yim. *J. Met.* **11**, 2, 304 (2021). <https://doi.org/10.3390/met11020304>
- [24] J. Oh, H. Choi-Yim. *J. Korean Phys. Soc.* **69**, 12, 1813 (2016). <http://dx.doi.org/10.3938/jkps.69.1813>
- [25] N.V. Ershov, V.I. Fedorov, Yu.P. Chernenkov, V.A. Lukshina, D.A. Shishkin. *FTT* **59**, 9, 1724 (2017) (in Russian). <http://dx.doi.org/10.21883/FTT.2017.09.44843.078>
- [26] M. Veligatla, S. Katakam, S. Das, N. Dahotre, R. Gopalan, D. Prabhu, D.A. Babu, H. Choi-Yim, S. Mukherjee. *Met. Mater. Trans. A* **46**, 3, 1019 (2015). <http://dx.doi.org/10.1007/s11661-014-2714-2>
- [27] C.-S. Yoo, S.K. Lim, C.S. Yoon, C.K. Kim. *J. Alloys Compd.* **359**, 1–2, 261 (2003). [http://dx.doi.org/10.1016/S0925-8388\(03\)00177-4](http://dx.doi.org/10.1016/S0925-8388(03)00177-4)
- [28] D. Huang, Y. Li, Y. Yang, Z. Zhu, W. Zhang. *J. Alloys Compd.* **843**, 154862 (2020). <https://doi.org/10.1016/j.jallcom.2020.154862>
- [29] Z.J. Yan, B.R. Bian, Y. Hu, S.E. Dang, L.T. Xia, Y.M. Wang. *J. Magn. Magn. Mater.* **322**, 21, 3359 (2010). <http://dx.doi.org/10.1016/j.jmmm.2010.06.027>

- [30] D. Muraca, V. Cremaschi, J. Moya, H. Sirkin. *J. Magn. Magn. Mater.* **320**, 9, 1639 (2008).
<http://dx.doi.org/10.1016/j.jmmm.2008.01.034>
- [31] V. Cremaschi, A. Saad, J. Moya, B. Arcondo, H. Sirkin. *Phys. B: Condens. Matter* **320**, 1–4, 281 (2002).
[https://doi.org/10.1016/S0921-4526\(02\)00715-9](https://doi.org/10.1016/S0921-4526(02)00715-9)
- [32] S. Kwon, S. Kim, H. Choi-Yim. *J. Korean Phys. Soc.* **72**, 1, 171 (2018). <http://dx.doi.org/10.3938/jkps.72.171>
- [33] G.E. Abrosimova, I.M. Shmytko. *Zav. labor. Diagnostika materialov*, **84** 6, 34 (2018) (in Russian).
<http://dx.doi.org/10.26896/1028-6861-2018-84-6-34-37>
- [34] G.E. Abrosimova, N.A. Volkov, E.A. Pershina, V.V. Chirkova, I.A. Sholin, A.S. Aronin. *J. Non-Cryst. Solids* **565**, 120864 (2021). <https://doi.org/10.1016/j.jnoncrysol.2021.120864>
- [35] Ł. Madej, L. Bednarska, V. Nosenko, B. Kotur, A. Chrobak, G. Hanezok. *Chem. Met. Alloys* **1**, 3/4, 333 (2008).
<http://dx.doi.org/10.30970/cma1.0072>
- [36] N.V. Ilyin, V.S. Komogortsev, G.S. Kraynova, V.A. Ivanov, I.A. Tkachenko, V.V. Tkachev, V.S. Plotnikov, R. S. Iskhakov. *Izv. RAN. Ser. fiz.* **85**, 9, 1234 (2021) (in Russian).
<https://doi.org/10.31857/S0367676521090143>
- [37] A. Lovas, L.F. Kiss, I. Balogh. *J. Magn. Magn. Mater.* **215–216**, 463 (2000).
[https://doi.org/10.1016/S0304-8853\(00\)00189-X](https://doi.org/10.1016/S0304-8853(00)00189-X)
- [38] H. Atmani, S. Grognet, J. Teillet. *J. Non-Cryst. Solids* **290**, 2–3, 194 (2001).
[https://doi.org/10.1016/S0022-3093\(01\)00737-2](https://doi.org/10.1016/S0022-3093(01)00737-2)
- [39] J. Han, S. Kwon, S. Sohn, J. Schroers, H. Choi-Yim. *J. Met.* **10**, 10, 1297 (2020). <https://doi.org/10.3390/met10101297>
- [40] C.C. Tsuei, H. Lilienthal. *Phys. Rev. B Condens. Matter* **13**, 11, 4899 (1976). <https://doi.org/10.1103/PhysRevB.13.4899>
- [41] L.M. Bednarska, Yu.K. Horelenko, M.O. Kovbuz, O.M. Hertsyk, B.Ya. Kotur, V.K. Nosenko. *Mater. Sci.* **39**, 2, 291 (2003).
<http://dx.doi.org/10.1023/B:MASC.0000010283.76730.8b>
- [42] R. Onodera, S. Kimura, K. Watanabe, S. Lee, Y. Yokoyama, A. Makino, K. Koyama. *Mater. Trans.* **54**, 2, 188 (2013).
<http://dx.doi.org/10.2320/matertrans.M2012242>
- [43] H.J. Ma, J.T. Zhang, G.H. Li, W.X. Zhang, W.M. Wang. *J. Alloys Compd.* **501**, 2, 227 (2010).
<http://dx.doi.org/10.1016/j.jallcom.2010.04.075>
- [44] P. Vojtanič, R. Andrejco, R. Varga, J. Kováč, K. Csach, A. Lovas. *Czechoslov. J. Phys.* **54**, 4, 113 (2004).
<https://doi.org/10.1007/s10582-004-0042-2>
- [45] G. Abrosimova, N. Volkov, V. Chirkova, A. Aronin. **297**, 129996 (2021). <https://doi.org/10.1016/j.matlet.2021.129996>